# Data-driven Distributionally Robust Co-optimization of P2P Energy Trading and Network Operation for Interconnected Microgrids

Jiayong Li, *Member, IEEE*, Mohammad E. Khodayar, *Senior Member, IEEE*, Jianhui Wang, *Fellow, IEEE*, Bin Zhou, *Senior Member, IEEE*

***Abstract*—This paper proposes a data-driven distributionally robust co-optimization model for the peer-to-peer (P2P) energy trading and network operation of interconnected microgrids (MGs). In particular, three-phase unbalanced MG networks are considered to account for the implementation practices, and the emerging soft open point (SOP) technology is used for the flexible connection of the multi-MGs. First, the energy management in individual MGs is modeled as a distributionally robust optimization (DRO) problem considering the P2P energy trading options and various operational constraints. Later, a novel decentralized and incentive-compatible pricing strategy is developed for P2P energy trading using the alternating direction method of multipliers (ADMM). Furthermore, the uncertainties in load consumption and renewable generation (RG) are taken into account and the Wasserstein metric (WM) is used to construct the ambiguity set of the uncertainty probability distributions (PDs). Consequently, only historical data is needed rather than prior knowledge about the actual PDs. Finally, the equivalent linear programming reformulations are derived for the DRO model to achieve computational tractability. Numerical tests on four interconnected MGs corroborate the advantages of the proposed P2P energy trading scheme and also demonstrate that the proposed DRO model is more effective in handling the uncertainties compared to the robust optimization (RO) and the stochastic programming (SP) models.**

***Index Terms*—Distributionally robust optimization, decentralized pricing approach, networked microgrids, peer-to-peer energy trading.**

## NOMENCLATURE

**Parameters**:

$\boldsymbol{p}^{\mathrm{L}}_{i,t}/\boldsymbol{q}^{\mathrm{L}}_{i,t}$ Active/reactive load at bus $i$

$\beta^{\mathrm{DG}}_{i,g}/\beta^{\mathrm{RG}}_{i,k}$ Binary parameter indicating whether DG $g$ /RG $k$ is located at bus $i$

$\beta^{\mathrm{ES}}_{i,b}$ Binary parameter indicating whether BES $b$ is located at bus $i$

$\beta^{n}_{i,m}$ Binary parameter indicating whether bus $i$ is one terminal of the SOP interconnecting MGs $m$ and $n$

$\underline{p}^{\mathrm{DG}}_{\phi,g,t}/\overline{p}^{\mathrm{DG}}_{\phi,g,t}$ Lower/upper bound of active power for DG $g$ in phase $\phi$

$\underline{q}^{\mathrm{DG}}_{\phi,g,t}/\overline{q}^{\mathrm{DG}}_{\phi,g,t}$ Lower/upper bound of reactive power for DG $g$ in phase $\phi$

$\underline{q}^{\mathrm{RG}}_{\phi,k,t}/\overline{q}^{\mathrm{RG}}_{\phi,k,t}$ Lower/upper bound of reactive power for RG $k$ in phase $\phi$

$\overline{p}^{\mathrm{C}}_{\phi,b,t}/\overline{p}^{\mathrm{D}}_{\phi,b,t}$ Maximum charging/discharging power for BES $b$ in phase $\phi$

$\eta^{\mathrm{C}}_{b}/\eta^{\mathrm{D}}_{b}$ Charging/discharging efficiency of BES $b$

$c^{1}_{g\kappa}/c^{0}_{g\kappa}$ Linear/constant generation cost coefficient for segment $\kappa$ of DG $g$

$\hat{\omega}_{\phi,j}$ Total power deviation in phase $\phi$ of sample $j$

**Variables**:

$\boldsymbol{p}^{\mathrm{DG}}_{g,t}/\boldsymbol{q}^{\mathrm{DG}}_{g,t}$ Active/reactive power output of DG $g$

$\boldsymbol{p}^{\mathrm{RG}}_{k,t}/\boldsymbol{q}^{\mathrm{RG}}_{k,t}$ Active/reactive power output of RG $k$

$\boldsymbol{p}^{\mathrm{D}}_{b,t}/\boldsymbol{p}^{\mathrm{C}}_{b,t}$ Discharging/charging power of BES $b$

$\boldsymbol{P}^{m}_{i,t}/\boldsymbol{Q}^{m}_{i,t}$ Active/reactive power flow on line $i$ in MG $m$

$\boldsymbol{p}^{n}_{m,t}$ Active power transferred from MG $n$ to MG $m$

$\boldsymbol{U}^{m}_{i,t}$ Squared nodal voltage magnitude at bus $i$ in MG $m$

$\boldsymbol{S}^{m}_{i,t}$ Apparent power flow on line $i$ in MG $m$

$\boldsymbol{\lambda}^{n}_{m,t}$ P2P energy trading price between MGs $m$ and $n$

$\overline{r}^{\mathrm{DG}}_{\phi,g,t}/\underline{r}^{\mathrm{DG}}_{\phi,g,t}$ Upward/Downward reserve of DG $g$ in phase $\phi$

$\overline{r}^{\mathrm{ES}}_{\phi,b,t}/\underline{r}^{\mathrm{ES}}_{\phi,b,t}$ Upward/Downward reserve of BES $b$ in phase $\phi$

$E_{b,t}$ State of charging (SOC) of BES $b$

$\alpha^{\mathrm{DG}}_{\phi,g,t}$ Affine participation factor of DG $g$ in phase $\phi$

$\alpha^{\mathrm{ES}}_{\phi,b,t}$ Affine participation factor of BES $b$ in phase $\phi$

$\Delta p^{\mathrm{DG}}_{\phi,g,t}$ Real-time power adjustment of DG $g$ in phase $\phi$

$\Delta p^{\mathrm{ES}}_{\phi,b,t}$ Real-time power adjustment of BES $b$ in phase $\phi$

$\hat{\boldsymbol{p}}^{n}_{m,t}$ Auxiliary variable duplicating the value of $\boldsymbol{p}^{n}_{m,t}$

The work of J. Li is supported by the National Natural Science Foundation of China under Grant No. 51907056. The work of B. Zhou is supported by the National Natural Science Foundation of China under Grant No. 51877072. The work of M. E. Khodayar is supported by the U.S. National Science Foundation under Grant ECCS-1710923.

J. Li and B. Zhou are with the College of Electrical and Information Engineering, Hunan University, Changsha 410082, China (email: j-y.li@connect.polyu.hk; binzhou@hnu.edu.cn).

M. E. Khodayar and J. Wang are with the Department of Electrical and Computer Engineering, Southern Methodist University, Dallas, TX 75275 USA (email: mkhodayar@smu.edu, jianhui@smu.edu).

## I. INTRODUCTION

MICROGRID (MG) has become the common practice for addressing various operation challenges stemming from the increase in the penetration level of distributed energy resources (DERs) such as photovoltaic (PV) panels [1]. Networking multiple self-governed MGs enables the power

exchange among the interconnected MGs and has been verified as an effective strategy to improve the overall reliability and resilience of the energy supply [2]. Conventionally, the operation of the networked MGs is supervised by the distribution network (DN) operator in a centralized manner [3], [4]. However, this operation scheme may lead to operational inefficiencies in MGs as they are owned and operated by private entities [2]. Although P2P energy trading could improve economic benefits to individual MGs, merely considering this economic objective could undermine the network operation performance by causing nodal over-voltage and under-voltage violations, as well as the voltage unbalance. Therefore, it is imperative to resolve the economic issues in energy trading and the technical issues in MG operation in a holistic manner through joint optimization of P2P energy trading and network operation while preserving the privacy and autonomy of individual MGs.

One typical method for networking the multi-MGs is to interconnect them through the local DN [5], [6]. However, such connections have several drawbacks. First, the connection will be disrupted once a fault occurs on the distribution path between the interconnected MGs. Furthermore, the power flow between the interconnected MGs is not fully controllable as it follows Kirchhoff's laws. Thanks to the fast development in power electronics, the recently emerging soft open point provides a satisfactory alternative for the flexible connection of the multi-MGs [7]. The SOP is fully controllable as it is developed from two back-to-back voltage source converters. Moreover, the fault within each MG can be easily isolated due to the isolation of the DC link in an SOP. To fully leverage the advantages of SOP, further research is demanded to address the interactions among MGs.

The energy trading or sharing among the multi-MGs without considering the detailed connection modes has been investigated extensively [8]–[15]. In particular, earlier works merely focused on designing fair energy trading mechanisms and oversimplified the energy scheduling within each MG [8]–[11]. To name a few, a Nash bargaining-based energy trading scheme was proposed in [8] for multi-MGs, whereas each MG was simplified as a lumped node without considering the detailed network constraints. In [9], the energy trading problem among multi-MGs was solved by a distributed optimization approach, while the internal scheduling of each MG was reduced to a power balance equation. In [10], the authors developed a distributed transactive energy management scheme for multi-MGs. Nonetheless, network constraints were neglected. To overcome this drawback, recently, some efforts have been devoted to the joint optimization of energy trading and network operation [12]–[15]. For instance, in our previous work [12], we proposed a distributed transactive energy framework by seamlessly integrating a bilateral energy trading mechanism with the optimal operation of the DN. In [13], a sensitivity analysis-based method was incorporated to ensure that P2P energy transaction did not violate the network constraints. Ref. [14] formulated the energy trading among multi-MGs as a generalized Nash bargaining problem that involved the DN operational constraints. Nonetheless, all these mentioned works failed to account for the underlying uncertainties associated with the electricity demand and renewable generation.

To effectively handle the uncertainties, various approaches including stochastic programming [16]–[18], robust optimization [19], [20], and DRO [21], [22] have been developed in the literature. In [17], the energy sharing problem for the PV prosumers was modeled as an SP problem where the uncertainty of PV generation was represented by a group of scenarios generated using a predefined probability distribution function (PDF). In [18], the chance-constrained approach was applied to the joint P2P energy and reserve market where the uncertainty of the renewable generation was represented by a versatile PD. In [23], the demand uncertainty and upstream price uncertainty were considered in the proposed P2P energy trading market design, and a probabilistic strategy was developed to address the uncertainty. However, the accurate PDF of random variables is generally unknown and only limited historical data is available [24], [25]. On the contrary, RO only requires limited information regarding the support set of random variables [19]. In [20], RO was applied to the energy trading problem to tackle different types of uncertainties. In [26], a hybrid robust and stochastic approach was developed to handle the uncertainty of renewable energy resources in energy trading between MGs. However, since RO merely optimizes the objective for the worst-case scenarios, it inevitably leads to an over-conservative outcome.

The recently emerging DRO approach provides an excellent alternative to the SP and RO as it remedies the SP's susceptibility and RO's insensitivity to the probabilistic information [21]. In DRO, the true distribution of uncertainties lies in an ambiguity set with high confidence, and thus the obtained solution is immune to all distributions in the ambiguity set [21]. The Wasserstein metric-based DRO directly constructs the ambiguity set of PDs from the historical samples and therefore, it is considered as a data-driven approach. This approach was used in various applications and demonstrated improved performance compared to the SP and RO [27]–[31]. To name a few, in [27]–[29], the Wasserstein metric-based DRO approach was utilized to investigate the optimal power flow (OPF) problem in the transmission networks. In [31], a data-driven DRO model was proposed for the scheduling of a microgrid with hydrogen fueling stations. In [32], the unit commitment problem was formulated as a DRO model to mitigate the risk associated with the wind power forecast errors. Motivated by the outstanding merits of the Wasserstein metric-based DRO, this approach is adopted here to handle the uncertainties in P2P energy trading.

To sum up, most existing works e.g. [8]–[11], either did not consider the co-optimization of P2P energy trading and network operation or oversimplified the individual MG as a lumped node for the computation tractability. Furthermore, previous works preferred using SP or RO in handling the uncertainties in P2P energy trading. Nevertheless, as aforementioned, SP requires prior knowledge about the precise PDF of the uncertain variables and RO suffers from the over-conservativeness. Hence, DRO formulation is proposed to address the shortcomings of SP and RO. This paper endeavors to fill these gaps by proposing a data-driven distributionally robust model for the co-optimization of P2P energy trading and network operation in the multiple interconnected MGs.

In particular, three-phase unbalanced MGs are considered to account for the implementation practices and the detailed network constraints are represented by the linearized multi-phase DistFlow model. First, a DRO model is formulated for individual MGs to minimize the operation cost with the given P2P trading prices. Then, a novel decentralized pricing strategy is developed for P2P energy trading. Finally, the ambiguity set is constructed using the Wasserstein metric and linear programming reformulations are derived. The contributions of this paper are three-fold as follows:

- Unlike most of the existing works that merely focus on the energy trading mechanisms, a co-optimization model is proposed for the P2P energy trading and network operation in multi-MGs considering various operational constraints. The SOP technology is used for the flexible interconnection of multi-MGs. Here, MGs are considered as autonomous entities with three-phase unbalanced networks as opposed to most of the related works in which MGs are oversimplified as lumped nodes.
- The co-optimization problem is formulated as a data-driven DRO model to handle the uncertainties of load and renewable generation. This is the first effort to apply the data-driven DRO approach to the multi-MG energy trading and operation problem. The Wasserstein metric is employed to construct the ambiguity set and equivalent linear programming reformulations are derived for the DRO model to reduce computational complexity.
- A novel fully decentralized pricing scheme that is incentive-compatible is developed for P2P energy trading. A closed-form solution to the subproblem is derived to improve computational efficiency. Furthermore, the proposed pricing scheme achieves the minimum overall social cost.

The remainder of this paper is organized as follows. Section II introduces the problem formulation of energy management of three-phase unbalanced MGs incorporating P2P energy trading. In Section III, a decentralized pricing scheme is developed. In Section IV, the ambiguity set of uncertainty PDs is constructed using the Wasserstein metric and linear programming reformulations are provided for the DRO problem. Numerical results are demonstrated in Section V. Finally, Section VI concludes the paper.

## II. Problem Formulation

### A. Notations

The subscripts/superscripts $m$, $t$ and $\phi$ denote the indices of MGs, time intervals, and phases, respectively; their corresponding sets are represented by $\mathcal{M}$, $\mathcal{T}$ and $\Phi$, respectively. The subscripts $g$, $k$ and $b$ denote the indices of dispatchable distributed generation (DG), renewable generation and battery energy storage (BES) in each MG, and their corresponding sets are represented by $\mathcal{G}_m$, $\mathcal{K}_m$ and $\mathcal{B}_m$, respectively. We use bold letters to denote the vectors. For example, $\boldsymbol{p}^{\mathrm{DG}}_{g,t} = [p^{\mathrm{DG}}_{a,g,t}\ p^{\mathrm{DG}}_{b,g,t}\ p^{\mathrm{DG}}_{c,g,t}]^\top$ is a column vector of the 3-phase active power output of DG $g$. The frequently used notations in this paper are illustrated in the Nomenclature.

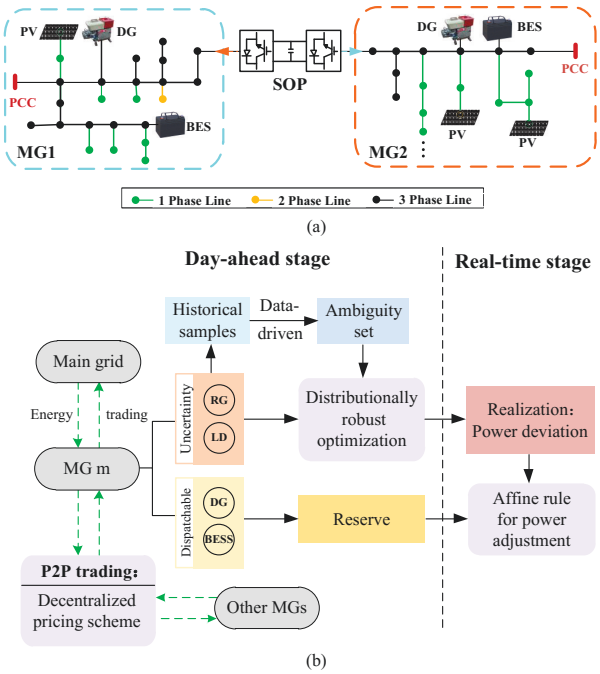


Fig. 1. (a) Example of two interconnected multi-phase unbalanced MGs (b) the illustration of the proposed co-optimization framework

Consider MG $m$ with a radial network as a connected tree $\mathcal{T}_m(\mathcal{N}_m, \mathcal{E}_m)$, where $\mathcal{N}_m := \{0, 1, ..., N\}$ and $\mathcal{E}_m$ represent the bus and line sets, respectively. The point of common couple (PCC) is indexed as 0. Each bus $i$ is directly connected to a unique parent bus $\pi_i$ and perhaps a set of child buses, denoted by $\Lambda_i$. The buses are labeled from the upstream buses to the downstream buses in the ascending order, i.e., $\pi_i < i$. Besides, the line pointing from the parent bus $\pi_i$ to bus $i$ is labeled as line $i$ and thus $\mathcal{E}_m := \{1, ..., N\}$.

### B. Energy Management in Each MG

Fig. 1(a) shows an example of two multi-phase unbalanced MGs that are interconnected through an SOP composed of two back-to-back voltage source converters. The power transferred through the SOP is fully controllable, and this lays a solid technical foundation for the P2P energy trade among the interconnected MGs. To promote P2P energy trading and ensure operational security and reliability, a data-driven distributionally robust co-optimization model of energy trading and network operation, is proposed for individual MGs. The overall illustration of the proposed framework is demonstrated in Fig. 1(b). As shown in the figure, each MG can either procure energy from the main grid at a given price or from the P2P trading at a contracted price. In this section, we temporally assume the P2P prices are known and will develop a decentralized pricing scheme to determine such prices in the next section. Furthermore, since the RG and load consumption (LD) are uncertain at the day-ahead (DA) stage, the data-driven DRO approach is adopted to handle the uncertainties. Particularly, in the proposed data-driven approach, the true PDs of the uncertain variables are ambiguous and only historical samples are available for the

construction of the ambiguity sets. DGs and BESs in each MG are dispatched to minimize the operation cost for each MG and provide the upward/downward reserves at the DA stage to facilitate the real-time power adjustment after the realization of uncertainties.

*1) System Model:* The linearized multiphase DistFlow model is adopted to describe the power flows in three-phase unbalanced MGs.

$$\boldsymbol{P}^m_{i,t}+\sum_{g\in\mathcal{G}_m}\beta^{\text{DG}}_{i,g}\cdot\boldsymbol{p}^{\text{DG}}_{g,t}+\sum_{k\in\mathcal{K}_m}\beta^{\text{RG}}_{i,k}\cdot\boldsymbol{p}^{\text{RG}}_{k,t}+\sum_{n\in\mathcal{M}\setminus m}\beta^{n}_{i,m}\cdot\boldsymbol{p}^{n}_{m,t}+\sum_{b\in\mathcal{B}_m}\beta^{\text{ES}}_{i,b}\cdot(\boldsymbol{p}^{\text{D}}_{b,t}-\boldsymbol{p}^{\text{C}}_{b,t})-\boldsymbol{p}^{\text{L}}_{i,t}=\sum_{j\in\Lambda_i}\boldsymbol{P}^m_{j,t} \tag{1a}$$

$$\boldsymbol{Q}^m_{i,t}+\sum_{g\in\mathcal{G}_m}\beta^{\text{DG}}_{i,g}\cdot\boldsymbol{q}^{\text{DG}}_{g,t}+\sum_{k\in\mathcal{K}_m}\beta^{\text{RG}}_{i,k}\cdot\boldsymbol{q}^{\text{RG}}_{k,t}-\boldsymbol{q}^{\text{L}}_{i,t}=\sum_{j\in\Lambda_i}\boldsymbol{Q}^m_{j,t} \tag{1b}$$

$$\boldsymbol{U}^m_{\pi_i,t}-\boldsymbol{U}^m_{i,t}=2\text{Re}\left(\tilde{\boldsymbol{z}}^*_{m,i}\boldsymbol{S}^m_{i,t}\right)\quad\forall i\in\mathcal{E}_m \tag{1c}$$

$$\underline{\boldsymbol{U}}^m_i\le\boldsymbol{U}^m_{i,t}\le\overline{\boldsymbol{U}}^m_i\quad\forall i\in\mathcal{N}_m \tag{1d}$$

$$\max_{\phi\in\Phi}\left|U^m_{\phi,i,t}-\frac{U^m_{a,i,t}+U^m_{b,i,t}+U^m_{c,i,t}}{3}\right|\le\epsilon\quad\forall i\in\mathcal{N}_m \tag{1e}$$

Constraints (1a) and (1b) represent the active and reactive power balance at each bus. The voltage drop on the distribution line is enforced by (1c), where $\tilde{\boldsymbol{z}}^*_{m,i}$ is a $3\times3$ complex matrix that represents the converted line impedance. For the detailed derivation of (1c) and the structure of the matrix $\tilde{\boldsymbol{z}}^*_{m,i}$, the interested reader is referred to Ref [33]. Here, (1d) imposes the upper and lower limits on the nodal voltage magnitudes and (1e) ensures that the voltage unbalance rate [34] at each bus does not exceed the upper limit $\epsilon$.

At the DA stage, each MG decides the energy transaction quantity with the main grid and other interconnected MGs. As seen from (1a), the active power exchange between MG $m$ and the main grid at time $t$ is $\boldsymbol{P}^m_{0,t}$. Hence, the cost (profit) of MG $m$ for buying (selling) energy from (to) the main grid in the time interval $t$ is expressed in (2), where $\lambda^b_t$ ($\lambda^s_t$) is the price for buying (selling) energy from (to) the main grid and $(\cdot)^+$ denotes a projection operator, i.e. $(x)^+=\max(x,0)$. Generally, $\lambda^b_t$ is higher than $\lambda^s_t$ [8].

$$\Omega^{m,1}_t\left(\boldsymbol{P}^m_{0,t}\right)=\lambda^b_t\cdot(\mathbf{1}^\top\boldsymbol{P}^m_{0,t}\Delta t)^+-\lambda^s_t\cdot(-\mathbf{1}^\top\boldsymbol{P}^m_{0,t}\Delta t)^+ \tag{2}$$

Likewise, the cost (profit) of MG $m$ for P2P energy trading at time interval $t$ is represented by (3).

$$\Omega^{m,2}_t\left(\boldsymbol{p}^n_{m,t}\right)=\sum_{n\in\mathcal{M}\setminus m}(\boldsymbol{\lambda}^n_{m,t})^\top\boldsymbol{p}^n_{m,t}\Delta t \tag{3}$$

*2) DG and RG Operation Constraints:* At the DA stage, the pre-dispatch of energy and reserve is decided for DGs to minimize the overall operation cost and to ensure the generation adequacy for the real-time adjustment. The operation constraints for each DG ($\forall g\in\mathcal{G}_m$) are presented in (4). Constraint (4a) ensures that the active power of DG minus the downward reserve does not fall below the lower bound of the active power output. Constraint (4b) guarantees that the active power of DG plus the upward reserve does not exceed the upper bound of the active power output. Here, (4c) illustrates that the reserves are non-negative; (4d) imposes the limits on the reactive power of each DG; and (4e) ensures that the power unbalance rate at each 3-phase DG does not exceed its tolerance $\delta_g$.

$$p^{\text{DG}}_{\phi,g,t}-\underline{r}^{\text{DG}}_{\phi,g,t}\ge\underline{p}^{\text{DG}}_{\phi,g}\quad\forall\phi\in\Phi \tag{4a}$$

$$p^{\text{DG}}_{\phi,g,t}+\overline{r}^{\text{DG}}_{\phi,g,t}\le\overline{p}^{\text{DG}}_{\phi,g}\quad\forall\phi\in\Phi \tag{4b}$$

$$\overline{r}^{\text{DG}}_{\phi,g,t}\ge0,\quad\underline{r}^{\text{DG}}_{\phi,g,t}\ge0\quad\forall\phi\in\Phi \tag{4c}$$

$$\underline{q}^{\text{DG}}_{\phi,g}\le q^{\text{DG}}_{\phi,g,t}\le\overline{q}^{\text{DG}}_{\phi,g}\quad\forall\phi\in\Phi \tag{4d}$$

$$\sum_{\phi,\psi,\phi\neq\psi}\left(|p^{\text{DG}}_{\phi,g,t}-p^{\text{DG}}_{\psi,g,t}|+|q^{\text{DG}}_{\phi,g,t}-q^{\text{DG}}_{\psi,g,t}|\right)\le\delta_g \tag{4e}$$

The active power outputs of RGs are assumed to be maintained at the maximum power point to harvest as much renewable energy as possible. The reactive power outputs of RGs are maintained within the feasible ranges as enforced by (5).

$$\underline{q}^{\text{RG}}_{\phi,k,t}\le q^{\text{RG}}_{\phi,k,t}\le\overline{q}^{\text{RG}}_{\phi,k,t}\quad\forall\phi\in\Phi_k,k\in\mathcal{K}_m \tag{5}$$

*3) BES Operation Constraints:* The pre-scheduling of energy and reserve for BES is also implemented at the DA stage. The operation constraints for each BES ($\forall b\in\mathcal{B}_m$) are introduced as,

$$p^{\text{C}}_{\phi,b,t}\ge0,\quad p^{\text{D}}_{\phi,b,t}\ge0,\quad\underline{r}^{\text{ES}}_{\phi,b,t}\ge0,\quad\overline{r}^{\text{ES}}_{\phi,b,t}\ge0 \tag{6a}$$

$$p^{\text{C}}_{\phi,b,t}+\underline{r}^{\text{ES}}_{\phi,b,t}\le\overline{p}^{\text{C}}_{\phi,b,t}\quad\forall\phi\in\Phi_b \tag{6b}$$

$$\underline{r}^{\text{ES}}_{\phi,b,t}\le\overline{p}^{\text{C}}_{\phi,b,t}+p^{\text{D}}_{\phi,b,t}\quad\forall\phi\in\Phi_b \tag{6c}$$

$$p^{\text{D}}_{\phi,b,t}+\overline{r}^{\text{ES}}_{\phi,b,t}\le\overline{p}^{\text{D}}_{\phi,b,t}\quad\forall\phi\in\Phi_b \tag{6d}$$

$$\overline{r}^{\text{ES}}_{\phi,b,t}\le\overline{p}^{\text{D}}_{\phi,b,t}+p^{\text{C}}_{\phi,b,t}\quad\forall\phi\in\Phi_b \tag{6e}$$

$$E_{b,t}=E_{b,t-1}+\sum_{\phi\in\Phi_b}\left(\eta^{\text{C}}_b\cdot p^{\text{C}}_{\phi,b,t}-p^{\text{D}}_{\phi,b,t}/\eta^{\text{D}}_b\right)\cdot\Delta t \tag{6f}$$

$$\underline{E}_b\le E_{b,t}\le\overline{E}_b \tag{6g}$$

$$E_{b,T}=E_{b,0} \tag{6h}$$

Constraint (6a) indicates the charging and discharging powers, as well as the downward and upward reserves, are non-negative. Constraint (6b) illustrates that the charging power plus the downward reserve should not exceed the maximum charging power when BES is in a charging state. Furthermore, (6c) shows that the upper bound of the downward reserve for BES unit is the maximum charging power plus the discharging power when BES is in discharging state. Similarly, (6d) guarantees that the discharging power plus the upward reserve does not exceed the maximum discharging power when BES is in discharging state. Constraint (6e) imposes the upper bound on the upward reserve when BES is in a charging state and (6f) shows the temporal variation of the SOC of BES $b$. Finally, (6g) imposes the limits on the SOC and (6h) indicates that the SOC at the end of the day is equal to the SOC at the beginning of the day.

To avoid over-exploitation of BES, the degradation cost of BES is included. Here, the degradation cost is formulated as a linear function of charging and discharging power as shown in (7), where $\theta_b$ is the cost coefficient associated with the lifetime degradation of the BES $b$ [17].

$$\Omega^{m,3}_t\left(\boldsymbol{p}^{\text{C}}_{b,t},\boldsymbol{p}^{\text{D}}_{b,t}\right)=\sum_{b\in\mathcal{B}_m,\phi\in\Phi_b}\theta_b\cdot(\eta^{\text{C}}_b\cdot p^{\text{C}}_{\phi,b,t}+p^{\text{D}}_{\phi,b,t}/\eta^{\text{D}}_b) \tag{7}$$

*4) SOP Operation Constraints:* To save the capacity for transferring active power and reduce the power loss, the reactive power generation/absorption by SOP is restrained. Constraint (8a) shows the power balance in each phase of SOP, where $p^{\text{Loss}}_{\phi,m,t}$ is the power loss on phase $\phi$ of SOP in MG $m$. Here, (8b) indicates that the power loss in SOP is linearly related to the power exchange, where $A^{\text{SOP}}_m$ is a very small constant (e.g. 0.02) which represents the loss coefficient [7], [35]. Furthermore, (8c) shows that the power exchange should not exceed the SOP capacity $S^{\text{SOP}}_{\phi,m}$.

$$p^n_{\phi,m,t} + p^{\text{Loss}}_{\phi,m,t} + p^m_{\phi,n,t} + p^{\text{Loss}}_{\phi,n,t} = 0 \quad \forall \phi \in \Phi \tag{8a}$$

$$p^{\text{Loss}}_{\phi,m,t} = A^{\text{SOP}}_m \cdot p^n_{\phi,m,t} \quad \forall \phi \in \Phi \tag{8b}$$

$$\left|p^n_{\phi,m,t}\right| \le S^{\text{SOP}}_{\phi,m} \quad \forall \phi \in \Phi \tag{8c}$$

*5) Affine Adjustment for the Uncertain Power Deviations:* After the realizations of uncertainties in RG and LD at the real-time stage, the reserves provided by DGs and BESs are deployed to maintain the power balance in each MG. Inspired by the AGC mechanism, affine rules for the power adjustment of DGs and BESs are adopted as (9).

$$\Delta p^{\text{DG}}_{\phi,g,t} = \alpha^{\text{DG}}_{\phi,g,t} \cdot \omega^m_{\phi,t} \quad \forall \phi \in \Phi, g \in \mathcal{G}_m \tag{9a}$$

$$\Delta p^{\text{ES}}_{\phi,b,t} = \alpha^{\text{ES}}_{\phi,b,t} \cdot \omega^m_{\phi,t} \quad \forall \phi \in \Phi, b \in \mathcal{B}_m \tag{9b}$$

$$0 \le \alpha^{\text{DG}}_{\phi,g,t} \le 1 \quad \forall \phi \in \Phi, g \in \mathcal{G}_m \tag{9c}$$

$$0 \le \alpha^{\text{ES}}_{\phi,b,t} \le 1 \quad \forall \phi \in \Phi, b \in \mathcal{B}_m \tag{9d}$$

$$\sum_{g \in \mathcal{G}_m} \alpha^{\text{DG}}_{\phi,g,t} + \sum_{b \in \mathcal{B}_m} \alpha^{\text{ES}}_{\phi,b,t} = 1 \quad \forall \phi \in \Phi \tag{9e}$$

$$-\underline{r}^{\text{DG}}_{\phi,g,t} \le \Delta p^{\text{DG}}_{\phi,g,t} \le \overline{r}^{\text{DG}}_{\phi,g,t} \quad \forall \phi \in \Phi, g \in \mathcal{G}_m \tag{9f}$$

$$-\underline{r}^{\text{ES}}_{\phi,b,t} \le \Delta p^{\text{ES}}_{\phi,b,t} \le \overline{r}^{\text{ES}}_{\phi,b,t} \quad \forall \phi \in \Phi, b \in \mathcal{B}_m \tag{9g}$$

Here, (9a) and (9b) show the affine rules for the power adjustments of DG and BES, where $\omega^m_{\phi,t}$ is a random variable representing the total power deviation on phase $\phi$ of MG $m$. Constraints (9c)-(9e) illustrate the restrictions on the participation factors. Moreover, (9f) and (9g) guarantee that the reserves provided by each DG and BES are within their capacities. We introduce penalties for the reserve violations; therefore, violating the upward and downward reserve constraints lead to load shedding and renewable generation curtailment, respectively. Thus, the penalty for the reserve violations on each phase $\phi$ at time interval $t$ is a function of decision variables and the uncertainty variable $\omega^m_{\phi,t}$. Such penalty is formulated in (10), where $\theta^{\text{U}}_t$ and $\theta^{\text{L}}_t$ are the unit cost for the load curtailment and renewable generation curtailment [27].

$$\begin{aligned}\Psi^m_{\phi,t} = \theta^{\text{U}}_t \Big[ \sum_{g \in \mathcal{G}_m} (\alpha^{\text{DG}}_{\phi,g,t}\omega^m_{\phi,t} - \overline{r}^{\text{DG}}_{\phi,g,t})^+ + \sum_{b \in \mathcal{B}_m} (\alpha^{\text{ES}}_{\phi,b,t}\omega^m_{\phi,t} - \overline{r}^{\text{ES}}_{\phi,b,t})^+ \Big] \\ + \theta^{\text{L}}_t \Big[ \sum_{g \in \mathcal{G}_m} (-\alpha^{\text{DG}}_{\phi,g,t}\omega^m_{\phi,t} - \underline{r}^{\text{DG}}_{\phi,g,t})^+ + \sum_{b \in \mathcal{B}_m} (-\alpha^{\text{ES}}_{\phi,b,t}\omega^m_{\phi,t} - \underline{r}^{\text{ES}}_{\phi,b,t})^+ \Big]\end{aligned} \tag{10}$$

Due to the affine power adjustment, the total generation cost of DG is represented as a function of uncertainties. The piece-wise linear generation cost function is adopted. With some mathematical manipulation, the total generation cost is reformulated as a piece-wise linear function of the uncertain variable $\boldsymbol{\omega}^m_t$ as shown in (11). Here, $\boldsymbol{\alpha}^{\text{DG}}_{g,t} := [\alpha^{\text{DG}}_{a,g,t}\ \alpha^{\text{DG}}_{b,g,t}\ \alpha^{\text{DG}}_{c,g,t}]^\top$; $c^1_{g\kappa}$ and $c^0_{g\kappa}$ are the cost coefficients for segment $\kappa$; $\boldsymbol{a}^{\text{DG}}_{\kappa,g,t} := c^1_{g\kappa} \cdot \boldsymbol{\alpha}^{\text{DG}}_{g,t}$ and $b^{\text{DG}}_{\kappa,g,t} := c^1_{g\kappa} \cdot \mathbf{1}^\top \boldsymbol{p}^{\text{DG}}_{g,t} + c^0_{g\kappa}$. Note that the adoption of piece-wise linear function is to reduce computational complexity. Even though the actual generation cost may not be linear like quadratic function, it could still be approximated by the piece-wise linear function.

$$\begin{aligned} f_{g,t}\big(\boldsymbol{p}^{\text{DG}}_{g,t}, \boldsymbol{\alpha}^{\text{DG}}_{g,t}, \boldsymbol{\omega}^m_t\big) &= \max_{\kappa \in \mathcal{K}_i} c^1_{g\kappa} \sum_{\phi \in \Phi} (p^{\text{DG}}_{\phi,g,t} + \Delta p^{\text{DG}}_{\phi,g,t}) + c^0_{g\kappa} \\ &= \max_{\kappa \in \mathcal{K}_i} (\boldsymbol{a}^{\text{DG}}_{\kappa,g,t})^\top \boldsymbol{\omega}^m_t + b^{\text{DG}}_{\kappa,g,t} \end{aligned} \tag{11}$$

Calling the reserve of BES at the real-time stage would cause deviation from the desired charging/discharging scheduling decisions at the DA stage. Thus, BES adjustment cost is introduced to quantify the unwillingness for this deviation. This cost is modeled as a linear function of the power deviation as formulated in (12), where $\boldsymbol{\alpha}^{\text{ES}}_{b,t} := [\alpha^{\text{ES}}_{\phi,b,t}]_{\phi \in \Phi_b}$; $\delta_{b,t}$ is the unit deviation cost for BES $b$ at time $t$; $\boldsymbol{a}^{\text{ES}}_{1,b,t} := \delta_{b,t} \cdot \boldsymbol{\alpha}^{\text{ES}}_{b,t}$ and $\boldsymbol{a}^{\text{ES}}_{2,b,t} = -\boldsymbol{a}^{\text{ES}}_{1,b,t}$.

$$h_{b,t}\big(\boldsymbol{\alpha}^{\text{ES}}_{b,t}, \boldsymbol{\omega}^m_t\big) = \delta_{b,t} \Big| \sum_{\phi \in \Phi_b} \Delta p^{\text{ES}}_{\phi,b,t} \Big| = \max_{\kappa \in \{1,2\}} (\boldsymbol{a}^{\text{ES}}_{\kappa,b,t})^\top \boldsymbol{\omega}^m_t \tag{12}$$

Let $\ell^m_t(\boldsymbol{x}^m_t, \boldsymbol{\omega}^m_t)$ denote the total cost associated with the uncertainties at time $t$, which is the summation of DG generation cost, BES adjustment cost and the penalty for reserve violations as shown in (13). Here, $\boldsymbol{x}^m_t$ collects the decision variables of MG $m$ at time $t$.

$$\ell^m_t(\boldsymbol{x}^m_t, \boldsymbol{\omega}^m_t) = \sum_{g \in \mathcal{G}_m} f_{g,t} + \sum_{b \in \mathcal{B}_m} h_{b,t} + \sum_{\phi \in \Phi} \Psi^m_{\phi,t} \tag{13}$$

*6) Distributionally Robust Energy Management Model in Each MG:* The overall operation cost of each MG can be divided into two parts such that the first part is associated with the decisions that are independent of the uncertainties and the second part is associated with the decisions affected by the imposed uncertainties. Thus, the objective of each MG is to minimize the energy procurement and battery degradation costs plus the expected total cost associated with the uncertainties considering the worst-case realization of the probability distributions as shown in (14). Here, $F^m_t(\boldsymbol{x}^m_t) := \Omega^{m,1}_t + \Omega^{m,3}_t$.

$$\min \sum_{t \in \mathcal{T}} \Big\{ F^m_t(\boldsymbol{x}^m_t) + \Omega^{m,2}_t + \sup_{\mathbb{P}_t \in \hat{\mathcal{P}}_t} \mathbb{E}_{\mathbb{P}_t} \Big[ \ell^m_t(\boldsymbol{x}^m_t, \boldsymbol{\omega}^m_t) \Big] \Big\} \tag{14a}$$

$$\begin{aligned} \text{over } \boldsymbol{x}^m_t := \Big\{ &\big(\boldsymbol{p}^{\text{DG}}_{g,t}, \boldsymbol{q}^{\text{DG}}_{g,t}, \underline{\boldsymbol{r}}^{\text{DG}}_{g,t}, \overline{\boldsymbol{r}}^{\text{DG}}_{g,t}, \boldsymbol{\alpha}^{\text{DG}}_{g,t}\big)_{g \in \mathcal{G}_m}, \big(\boldsymbol{q}^{\text{RG}}_{k,t}\big)_{k \in \mathcal{K}_m}, \\ &\big(\boldsymbol{p}^{\text{D}}_{b,t}, \boldsymbol{p}^{\text{C}}_{b,t}, \underline{\boldsymbol{r}}^{\text{ES}}_{b,t}, \overline{\boldsymbol{r}}^{\text{ES}}_{b,t}, \boldsymbol{\alpha}^{\text{ES}}_{b,t}\big)_{b \in \mathcal{B}_m}, \big(\boldsymbol{p}^n_{m,t}\big)_{n \in \mathcal{M} \setminus m}, \\ &\big(\boldsymbol{P}^m_{i,t}, \boldsymbol{Q}^m_{i,t}, \boldsymbol{U}^m_{i,t}\big)_{i \in \mathcal{N}_m} \Big\} \end{aligned}$$

$$\text{s.t. } (1), (4)\text{-}(6), (8c), (9a)\text{-}(9e) \quad \forall t \in \mathcal{T} \tag{14b}$$

## III. Decentralized Pricing Approach for P2P Energy Trading among Multi-MGs

In this section, first the energy management model for multi-MGs is formulated and then a novel decentralized pricing approach that achieves the minimum overall social cost is developed for the P2P energy trading. It is further validated that the proposed pricing approach is incentive compatible.

### A. Energy Management for Multi-MGs

The objective is to minimize the overall social cost that sums up the operation cost of individual MGs. Since the payments for P2P trading circulate within multi-MGs, they are canceled out in the objective function. The problem formulation for the energy management is shown in (15), where $\boldsymbol{x} = \{\boldsymbol{x}_t^m\}_{m\in\mathcal{M},t\in\mathcal{T}}$. Here, (15c) is simplified from (8a) by neglecting the power loss in SOP as it is relatively small compared with the power flow in the SOP.

$$\min_{\boldsymbol{x}} \sum_{m\in\mathcal{M}}\sum_{t\in\mathcal{T}} \left\{ F_t^m(\boldsymbol{x}_t^m) + \sup_{\mathbb{P}_t\in\hat{\mathcal{P}}_t} \mathbb{E}_{\mathbb{P}_t}\left[\ell_t^m(\boldsymbol{x}_t^m,\boldsymbol{\omega}_t^m)\right]\right\} \quad (15a)$$

$$\text{s.t. } (1),(4),(6),(8c),(9a)\text{-}(9e) \quad \forall t\in\mathcal{T}, m\in\mathcal{M} \quad (15b)$$

$$\boldsymbol{p}_{m,t}^n + \boldsymbol{p}_{n,t}^m = 0 \quad \forall t\in\mathcal{T}, m/n\in\mathcal{M}, m\neq n \quad (15c)$$

To derive the pricing algorithm, (15c) is reformulated as (16a)-(16b) by introducing an auxiliary variable $\hat{\boldsymbol{p}}_{m,t}^n$.

$$\hat{\boldsymbol{p}}_{m,t}^n + \hat{\boldsymbol{p}}_{n,t}^m = 0 \quad \forall t\in\mathcal{T}, m/n\in\mathcal{M}, m\neq n \quad (16a)$$

$$\boldsymbol{p}_{m,t}^n = \hat{\boldsymbol{p}}_{m,t}^n \quad \forall t\in\mathcal{T}, m/n\in\mathcal{M}, m\neq n \quad (16b)$$

### B. Decentralized Pricing Algorithm

From the economic perspective, the optimal Lagrangian multipliers (dual variables) associated with constraints (15c) represent the shadow prices for the P2P energy trading. To determine these prices, a fully decentralized optimization algorithm based on ADMM is developed. Let $\boldsymbol{y}_t^m$ denote the collection of auxiliary variables, i.e, $\boldsymbol{y}_t^m := \{\hat{\boldsymbol{p}}_{m,t}^n\}_{n\in\mathcal{M}\setminus m}$, and $\boldsymbol{\lambda}_{m,t}^n$ be the Lagrangian multiplier associated with (16b). The augmented Lagrangian can be formulated as (17).

$$\mathcal{L}(\boldsymbol{x},\boldsymbol{y},\boldsymbol{\lambda}) = \sum_{m\in\mathcal{M}}\sum_{t\in\mathcal{T}} \mathcal{L}_t^m(\boldsymbol{x}_t^m,\boldsymbol{y}_t^m,\boldsymbol{\lambda}_t^m) \quad (17)$$

where $\mathcal{L}_t^m(\boldsymbol{x}_t^m,\boldsymbol{y}_t^m,\boldsymbol{\lambda}_t^m) = F_t^m(\boldsymbol{x}_t^m) + \sup_{\mathbb{P}_t\in\hat{\mathcal{P}}_t} \mathbb{E}_{\mathbb{P}_t}\left[\ell_t^m(\boldsymbol{x}_t^m,\boldsymbol{\omega}_t^m)\right]$ $+ \sum_{n\in\mathcal{M}\setminus m}\left[(\boldsymbol{\lambda}_{m,t}^n)^\top(\boldsymbol{p}_{m,t}^n - \hat{\boldsymbol{p}}_{m,t}^n) + \frac{\rho}{2}\|\boldsymbol{p}_{m,t}^n - \hat{\boldsymbol{p}}_{m,t}^n\|_2^2\right]$ and $\boldsymbol{\lambda}_t^m := \{\boldsymbol{\lambda}_{m,t}^n\}_{n\in\mathcal{M}\setminus m}$.

Let $\tau$ denote the iteration index. Then, the iterative procedure of the proposed decentralized pricing algorithm can be summarized as follows.

*1) Update of $\boldsymbol{x}^m$:* Thanks to the decomposable structure of the augmented Lagrangian and the constraints (15b), $\boldsymbol{x}^m$ could be updated in a fully decentralized manner. Each MG $m$ solves the problem (18) to update its local variable $\boldsymbol{x}_t^m$ by fixing the auxiliary variable $\boldsymbol{y}_t^{m,\tau}$ and the Lagrangian multiplier $\boldsymbol{\lambda}_t^{m,\tau}$.

$$\boldsymbol{x}_t^{m,\tau+1} := \arg\min_{\boldsymbol{x}_t^m\in\mathcal{X}_t^m} \sum_{t\in\mathcal{T}} \mathcal{L}_t^m(\boldsymbol{x}_t^m,\boldsymbol{y}_t^{m,\tau},\boldsymbol{\lambda}_t^{m,\tau}) \quad (18)$$

After solving (18), each MG $m$ broadcasts $\boldsymbol{p}_{m,t}^{n,\tau+1}$ to MG $n$.

*2) Update of $\boldsymbol{y}^m$:* The auxiliary variable $\boldsymbol{y}$ is updated by solving problem (19).

$$\min_{\boldsymbol{y}} \mathcal{L}(\boldsymbol{x}^\tau,\boldsymbol{y},\boldsymbol{\lambda}^\tau) \quad (19a)$$

$$\text{s.t. } (16a) \quad (19b)$$

Note that in problem (19), each $\hat{\boldsymbol{p}}_{m,t}^n$ is only coupled with $\hat{\boldsymbol{p}}_{n,t}^m$ and the objective function is also decomposable. Thus, each pair of $\hat{\boldsymbol{p}}_{m,t}^n$ and $\hat{\boldsymbol{p}}_{n,t}^m$ can be solved from the following problem which is decomposed from problem (19).

$$\min_{\hat{\boldsymbol{p}}_{m,t}^n} -(\boldsymbol{\lambda}_{m,t}^n)^\top\hat{\boldsymbol{p}}_{m,t}^n - (\boldsymbol{\lambda}_{n,t}^m)^\top\hat{\boldsymbol{p}}_{n,t}^m + \frac{\rho}{2}\left\|\hat{\boldsymbol{p}}_{m,t}^n - \boldsymbol{p}_{m,t}^n\right\|_2^2 + \frac{\rho}{2}\left\|\hat{\boldsymbol{p}}_{n,t}^m - \boldsymbol{p}_{n,t}^m\right\|_2^2 \quad (20a)$$

$$\text{s.t. } (16a) \quad (20b)$$

Hence, the closed-form solution of $\hat{\boldsymbol{p}}_{m,t}^n$ can be derived as (21) by solving the KKT condition of (20). Thus, $\boldsymbol{y}^m$ can be locally updated by MG $m$ without a central coordinator. Upon receiving $\boldsymbol{p}_{n,t}^{m,\tau+1}$ and $\boldsymbol{\lambda}_{n,t}^{m,\tau}$, MG $m$ updates $\hat{\boldsymbol{p}}_{m,t}^n$ accordingly.

$$\hat{\boldsymbol{p}}_{m,t}^{n,\tau+1} = -\hat{\boldsymbol{p}}_{n,t}^{m,\tau+1} = \frac{\boldsymbol{p}_{m,t}^{n,\tau+1} - \boldsymbol{p}_{n,t}^{m,\tau+1}}{2} + \frac{\boldsymbol{\lambda}_{m,t}^{n,\tau} - \boldsymbol{\lambda}_{n,t}^{m,\tau}}{2\rho} \quad (21)$$

*3) Update of $\lambda^m$:*

$$\boldsymbol{\lambda}_{m,t}^{n,\tau+1} = \boldsymbol{\lambda}_{m,t}^{n,\tau} + \rho\big(\boldsymbol{p}_{m,t}^{n,\tau+1} - \hat{\boldsymbol{p}}_{m,t}^{n,\tau+1}\big) \quad (22)$$

MG $m$ locally performs the update of Lagrangian multipliers and then sends $\boldsymbol{\lambda}_{m,t}^{n,\tau+1}$ to MG $n$.

**Remark**: The original formulated multi-MG energy management problem (15) is in a multi-block structure, while the convergence of the multi-block ADMM cannot be guaranteed. Thus, the auxiliary variable $\hat{\boldsymbol{p}}_{m,t}^n$ is introduced to convert the original problem into an equivalent problem with dual-block structure by replacing the constraint (15c) with (16a) and (16b). The first block of variables includes the network operation decision and the energy trading decisions, and the second block of variables consists of the auxiliary variables. It has been verified in [36] that the two-block ADMM for solving convex problems globally converges.

It will be shown in the next section that the DRO problem (15) can be reformulated as a linear programming problem using the Wasserstein metric. Hence, the convergence of the ADMM algorithm is guaranteed. Furthermore, we have $\boldsymbol{\lambda}_{m,t}^n = \boldsymbol{\lambda}_{n,t}^m$ because of (21) and (22). Therefore, problem (18) is equivalent to problem (14) when the consensus constraint (16b) is satisfied. This implies that the converged solution represents a Nash equilibrium.

## IV. Reformulation Based on Wasserstein Metric

### A. Wasserstein Metric Based Ambiguity Set

To evaluate the expectation value of a random variable $\omega$, its PD is required. However, in practical applications, the true PD $\mathbb{P}$ is usually ambiguous and only a set of historical samples $\hat{\omega} := \{\hat{\omega}_1,\hat{\omega}_2,...,\hat{\omega}_N\}$ is available. In this paper, we use the Wasserstein metric to construct the ambiguity set $\hat{\mathcal{P}}_N$ as it has the following properties [21]: 1) out-of-sample performance guarantee, 2) asymptotic guarantee, which implies that the

ambiguity set converges to the true distribution as the number of samples tends to increase to infinity, 3) tractability, which indicates that a computationally tractable reformulation can be obtained.

Given a set of historical samples, an empirical PD $\hat{\mathbb{P}}_N = \frac{1}{N}\sum_{k=1}^{N}\delta_{\hat{\omega}_k}$ can be derived to estimate $\mathbb{P}$, where $\delta_{\hat{\omega}_k}$ denotes the Dirac measure of $\hat{\omega}_k$. Generally, the WM is a way to measure the "distance" between the estimated PD and the true PD, defined as (23). Here, $\Xi$ is the compact support of the random variable, and $\Pi$ is a joint distribution of $\omega$ and $\hat{\omega}$ with marginal PD $\mathbb{P}$ and $\hat{\mathbb{P}}_N$, respectively.

$$W(\hat{\mathbb{P}}_N, \mathbb{P}) = \inf_{\Pi}\Big\{\int_{\Xi^2}\|\omega - \hat{\omega}\|\Pi(d\omega, d\hat{\omega})\Big\} \tag{23}$$

Then the ambiguity set can be constructed as (24), where $\varepsilon(N)$ is the radius of the ambiguity set $\hat{\mathcal{P}}$ whose center is $\hat{\mathbb{P}}_N$.

$$\hat{\mathcal{P}} := \big\{W(\hat{\mathbb{P}}_N, \mathbb{P}) \le \varepsilon(N)\big\} \tag{24}$$

According to [28], $\varepsilon(N)$ is a function of the confidence level $\beta$ and the sample number $N$, which can be expressed as

$$\varepsilon(N) = D\sqrt{\frac{2}{N}\ln(\frac{1}{1-\beta})} \tag{25}$$

where $D$ is a constant that represents the diameter of the support of random variable. Interested reader is referred to [28] for the computation of $D$.

Another widely used metric in DRO is the KL divergence [37], [38]. Compared with the Wasserstein metric, the KL divergence is asymmetric and does not satisfy the triangle inequality. Besides, the KL divergence only considers the probabilities of the observed points, while the Wasserstein metric takes into account the vicinity of the support points. Furthermore, the Wasserstein metric-based ambiguity set contains all continuous and discrete PDs that are sufficiently close to the empirical one, while the KL divergence based ambiguity set may exclude continuous PDs.

### *B. Problem Reformulation*

For mathematical conciseness, the superscripts $m$ and $t$ will be dropped in the following. Furthermore, the worst-case expected cost is approximated by an upper bound through interchanging the maximum and summation as shown in (26). Here, the first two terms on the right-hand side represent the worst-case expected generation cost and the BES adjustment cost, and the last term is the worst-case expected penalty cost.

$$\begin{aligned}\sup_{\mathbb{P}\in\hat{\mathcal{P}}}\mathbb{E}_{\mathbb{P}}\Big[\ell(\boldsymbol{x},\boldsymbol{\omega})\Big] \le \sum_{g\in\mathcal{G}}\sup_{\mathbb{P}\in\hat{\mathcal{P}}}\mathbb{E}_{\mathbb{P}}\Big[f_g(\boldsymbol{x},\boldsymbol{\omega})\Big] + \\ \sum_{b\in\mathcal{B}}\sup_{\mathbb{P}\in\hat{\mathcal{P}}}\mathbb{E}_{\mathbb{P}}\Big[h_b(\boldsymbol{x},\boldsymbol{\omega})\Big] + \sum_{\phi\in\Phi}\sup_{\mathbb{P}\in\hat{\mathcal{P}}}\mathbb{E}_{\mathbb{P}}\Big[\Psi_\phi(\boldsymbol{x}_\phi,\omega_\phi)\Big]\end{aligned} \tag{26}$$

As the worst-case PDs of the right-hand side (RHS) may not be identical with the worst-case PD of the left-hand side (LHS), the RHS represents an upper bound for the LHS. It has been verified in [27] that interchanging the maximum and the summation would only introduce a small error. However, the overall computational complexity is reduced exponentially as the total number of pieces of the loss function is reduced considerably.

Given (11) and (12), the worst-case expected generation cost and BES adjustment cost can be generalized as (27).

$$\sup_{\mathbb{P}\in\hat{\mathcal{P}}}\mathbb{E}_{\mathbb{P}}\Big[\max_{1\le\kappa\le K}\boldsymbol{a}_\kappa^\top\boldsymbol{\omega} + b_\kappa\Big] \tag{27}$$

We assume that the support of $\boldsymbol{\omega}$ can be expressed as a polytope, i.e. $\Xi = \{\boldsymbol{\omega} : \boldsymbol{C\omega} \le \boldsymbol{d}\}$. Then, according to Corollary 5.1 in [21], the problem (27) admits a reformulation as (28). Here, $\hat{\boldsymbol{\omega}}_j$ is the $j$-th sample of $\boldsymbol{\omega}$. Note that $\boldsymbol{a}_\kappa$ and $b_\kappa$ are linear functions of $\boldsymbol{x}$. Therefore, (28) is a linear programming with respect to $\boldsymbol{x}$ and $\{\mu, s_j, \boldsymbol{\gamma}_{j\kappa}\}$.

$$\inf_{\mu, s_j, \boldsymbol{\gamma}_{j\kappa}} \mu\varepsilon + \frac{1}{N}\sum_{j=1}^{N} s_j \tag{28a}$$

$$\text{s.t. } b_\kappa + \boldsymbol{a}_\kappa^\top\hat{\boldsymbol{\omega}}_j + \boldsymbol{\gamma}_{j\kappa}^\top(\boldsymbol{d} - \boldsymbol{C}\hat{\boldsymbol{\omega}}_j) \le s_j \quad \forall j \le N, \kappa \le K \tag{28b}$$

$$\|\boldsymbol{C}^\top\boldsymbol{\gamma}_{j\kappa} - \boldsymbol{a}_\kappa\|_\infty \le \mu \quad \forall j \le N, \kappa \le K \tag{28c}$$

$$\boldsymbol{\gamma}_{j\kappa} \ge 0 \tag{28d}$$

Similarly, $\sup_{\mathbb{P}\in\hat{\mathcal{P}}}\mathbb{E}_{\mathbb{P}}\big[\Psi_\phi(\boldsymbol{x}_\phi, \omega_\phi)\big]$ can be reformulated as (29) according to Theorem 1 in [22].

$$\inf_{\nu_\phi, \zeta_{\phi,j}} \nu_\phi\varepsilon + \frac{1}{N}\sum_{j=1}^{N}\zeta_{j,\phi} \tag{29a}$$

$$\text{s.t. } \sup_{\omega_\phi\in[\underline{\omega}_\phi, \overline{\omega}_\phi]}\big(\Psi_\phi(\boldsymbol{x}_\phi, \omega_\phi) - \nu_\phi\big|\omega_\phi - \hat{\omega}_{\phi,j}\big|\big) \le \zeta_{j,\phi} \ \forall j \le N \tag{29b}$$

Since $\Psi_\phi(\boldsymbol{x}_\phi, \omega_\phi)$ is the point-wise supremum of some linear functions of $\omega_\phi$ according to (10), it is a convex function of $\omega_\phi$. Hence, the LHS of (29b) is to maximize a convex function over a compact interval. Therefore, the maximization is attained either on the boundaries ($\underline{\omega}_\phi$ and $\overline{\omega}_\phi$) or $\hat{\omega}_{\phi,j}$ and thus the problem (29) can be further rewritten as (30).

$$\inf_{\nu_\phi, \zeta_{\phi,j}} \nu_\phi\varepsilon + \frac{1}{N}\sum_{j=1}^{N}\zeta_{\phi,j} \tag{30a}$$

$$\text{s.t. } \Psi_\phi(\boldsymbol{x}_\phi, \underline{\omega}_\phi) + \nu_\phi\big(\underline{\omega}_\phi - \hat{\omega}_{\phi,j}\big) \le \zeta_{j,\phi} \quad \forall j \le N \tag{30b}$$

$$\Psi_\phi(\boldsymbol{x}_\phi, \overline{\omega}_\phi) - \nu_\phi\big(\overline{\omega}_\phi - \hat{\omega}_{\phi,j}\big) \le \zeta_{j,\phi} \quad \forall j \le N \tag{30c}$$

$$\Psi_\phi(\boldsymbol{x}_\phi, \hat{\omega}_{\phi,j}) \le \zeta_{j,\phi} \quad \forall j \le N \tag{30d}$$

Likewise, problem (30) is a linear programming with respect to $\boldsymbol{x}$ and $\{\nu_\phi, \zeta_{\phi,j}\}$. Therefore, both problems (15) and (18) can be reformulated as linear programming problems by replacing $\sup_{\mathbb{P}\in\hat{\mathcal{P}}}\mathbb{E}_{\mathbb{P}}\Big[\ell(\boldsymbol{x},\boldsymbol{\omega})\Big]$ with (28) and (30).

### *C. Implementation*

Algorithm 1 summarizes the distributed algorithm for solving the co-optimization of P2P energy trading and MG operation with a decentralized pricing scheme based on the ADMM approach. The first step is to initialize the auxiliary variables and the Lagrangian multipliers also known as the P2P energy trading prices. Then the iterative process begins at the 2nd step until the primal and dual residuals fall below the tolerance level at the 9th step. During the iteration, each MG $m$ cyclically updates the primal variables, auxiliary variable,

**Algorithm 1:** Distributed algorithm for solving the co-optimization of P2P energy trading and MG operation

Initialize $\hat{\boldsymbol{p}}^{n}_{m,t}$ and $\boldsymbol{\lambda}^{n}_{m,t}$ for all $m \in \mathcal{M}$, $n \in \mathcal{M} \backslash m$, $t \in \mathcal{T}$. Set the convergence tolerance level $\varepsilon_1$. Initialize the iteration index, i.e. $\tau = 0$ ;
**repeat**
  **for** $m = 1$ **to** $|\mathcal{M}|$ **do**
    Each MG $m$ updates the primal variables $\mathbf{x}^{m,\tau}_{i,t}$ according to (18) by jointly solving the reformulated DRO problem (28) and (30);
    Each MG $m$ updates the auxiliary variables $\boldsymbol{y}^{m,\tau}_{t}$, i.e. $\{\hat{\boldsymbol{p}}^{n,\tau}_{m,t}\}_{n \in \mathcal{M} \backslash m}$ according to (21);
    Each MG $m$ updates the Lagrangian multipliers $\boldsymbol{\lambda}^{n,\tau}_{m,t}$ according to (22);
    Update the iteration index $\tau = \tau + 1$;
  **end**
**until** $\max\left(\|\boldsymbol{p}^{n,\tau}_{m,t} - \hat{\boldsymbol{p}}^{n,\tau}_{m,t}\|\right) \leq \varepsilon_1$ **and** $\max\left(\rho\|\hat{\boldsymbol{p}}^{n,\tau}_{m,t} - \hat{\boldsymbol{p}}^{n,\tau-1}_{m,t}\|\right) \leq \varepsilon_1$;

and Lagrangian multipliers. The primal variables include the energy trading and MG operation decisions which are renewed at the 4th step. The auxiliary variables and the Lagrangian multipliers are updated at the 5th and 6th steps, respectively.

## V. Numerical Results

The proposed DRO model for the co-optimization of P2P energy trading and network operation is tested on four interconnected 3-phase unbalanced MGs which are constructed from the IEEE 123-bus DN as shown in Fig 2. The line parameters and the load data can be obtained from [39]. The locations of DERs and the boundaries of the MGs are indicated in Fig. 2. The capacities of 3-phase and single-phase PV units are 300 $kW$ and 100 $kW$, respectively. The power and energy capacities of each BES are 100 $kW$ and 1000 $kWh$, respectively. The capacity of each DG and wind turbine (WT) are 300 $kW$ and 500 $kW$, respectively. Without the loss of generality, the energy purchasing price from the main grid is set as $\$0.08/kWh$ during the off-peak periods (11:00 p.m.-6:00 a.m.) and $\$0.1/kWh$ during other periods, and the selling price is set as $\$0.04/kWh$. Furthermore, like Refs [27], [28], the samples generated from the predefined PDs are used in the case studies to represent the empirical data without loss of generality. The prediction errors of PV, wind, and loads are represented by Gaussian distributions with zero means. The standard deviations (SDs) for the PV and wind power prediction errors are set as $10\%$ of the predicated outputs and the SDs for the load prediction errors are set as $5\%$ of the nominal values. Three cases are considered to verify the effectiveness of the proposed framework. In the first case, the advantages of P2P energy trading are corroborated as well as the effectiveness of the proposed decentralized pricing scheme. In the second one, the merits of the co-optimization of P2P energy trading and network operation are validated through comparison with a scheme that only conducts P2P energy trading. In the last one, the performance of DRO is compared with three benchmarks. All tests are performed using MATLAB on a PC with an Intel Core i7 of 2.5GHz and 16GB memory.

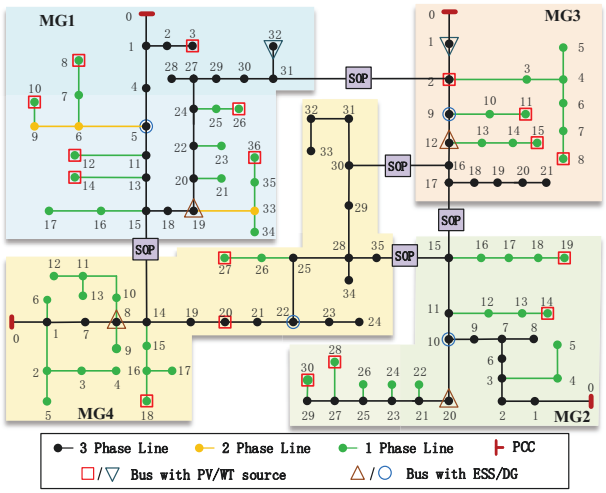


Fig. 2. Four interconnected 3-phase unbalanced microgrids constructed from IEEE 123-bus distribution network

TABLE I
Total Energy Procurement Cost/Profit of Each Microgrid with/without P2P Energy Trading

| | Total energy cost/profit ($) | | Cost reduction ($) |
|---|---|---|---|
| | Without P2P trading | With P2P trading | |
| MG1 | 28.5 | −87.7 | 116.2 |
| MG2 | 1475.7 | 1192.8 | 282.9 |
| MG3 | −330.7 | −692.0 | 361.3 |
| MG4 | 1416.3 | 1248.0 | 168.3 |
| Total | 2589.8 | 1661.1 | 928.7 |

### A. Effectiveness of Proposed P2P Trading and Pricing Scheme

In this subsection, the effectiveness of the P2P energy trading and the proposed decentralized pricing scheme is validated. Fig. 3 shows the energy procurement of each MG during the DA planning. Here, the negative values in the sub-figures indicate that the energy is sold to other entities. As shown in the figure, the energy surplus of MG1 is sold to MG4, and MG3 sells the majority of its excess energy to MG2 and the rest to MG4. Besides, during hours 9-16 when PV generation is high, the local energy supply within the multi-MGs is sufficient to serve all loads and both buyers (MG2 and MG4) acquire all their energy through the P2P trading. This implies that MGs prefer P2P trading over the transaction with the main grid. Table I summarizes the energy procurement cost/profit of each MG with and without P2P trading. As shown, implementing the P2P trading is beneficial to all MGs. Furthermore, the total cost is reduced by more than 35% which highlights the economical advantages of the proposed P2P energy trading scheme.

Fig. 4 depicts the corresponding P2P trading prices derived through the proposed decentralized pricing scheme as well as the prices for buying/selling energy from/to the main grid, denoted by $\lambda_b$ and $\lambda_s$, respectively. The P2P price between MG $i$ and MG $j$ is denoted by $\lambda_{ij}$. The results demonstrate that

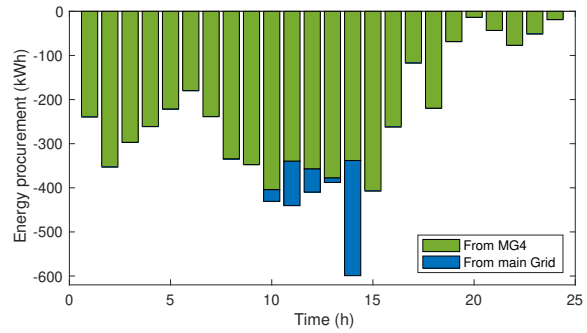


(a) MG1

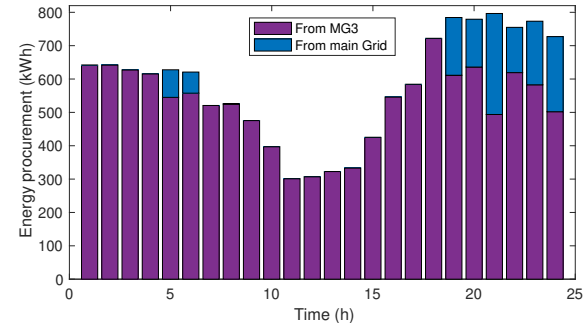


(b) MG2

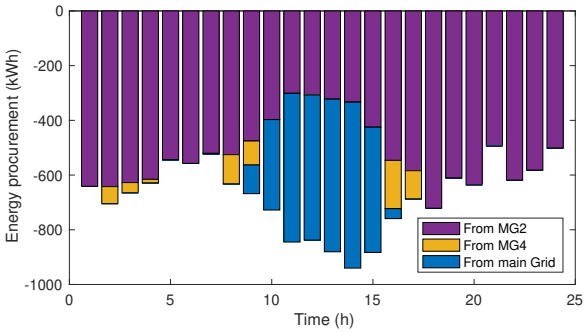


(c) MG3

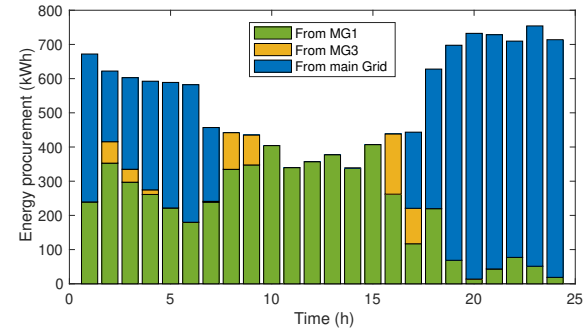


(d) MG4

Fig. 3. Energy procurement (a) MG1 (b) MG2 (c) MG3 (d) MG4

the P2P prices for all three phases are identical since the power exchange through the SOP does not reach the upper limit. We can observe from Fig. 4 that the P2P prices are within the interval $[\lambda_s, \lambda_b]$. Consequently, both the energy sellers and buyers are better off by participating in the P2P trading, which verifies that the proposed pricing strategy is incentive compatible. Besides, since $\lambda_{32}$ is higher than $\lambda_{34}$, MG3 prefers

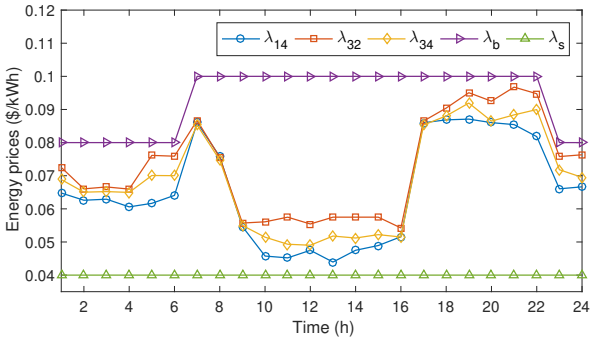


Fig. 4. Hourly prices for P2P energy trading among 4 interconnected MGs and prices for buying/selling energy from/to the main grid

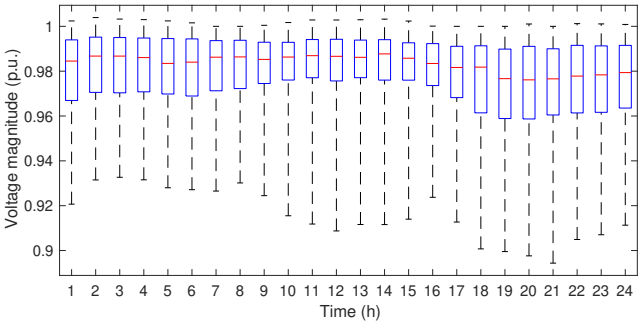


Fig. 5. Distribution of nodal voltage magnitudes under the scheme only considering P2P energy trading

selling energy to MG2 over MG4 and thus MG3 provides the excessive energy to MG4 only when the demand in MG2 is satisfied as shown by Figs. 3(b) and 3(c). Likewise, since $\lambda_{14}$ is lower than $\lambda_{34}$, MG4 prefers procuring energy from MG1 over MG3. Thus, the first choice of energy procurement to MG4 is from MG1 and the last choice is from the main grid as shown by Fig. 3(d). Moreover, Fig. 4 indicates that the P2P prices are inversely correlated with the total available generation within the interconnected MGs. Specifically, they are high when the total generation is insufficient, and low when the local generation is abundant, which further validates the effectiveness of the proposed decentralized pricing scheme.

### *B. Merits of Co-optimization Strategy*

To demonstrate the merits of the proposed co-optimization scheme over the benchmark scheme that only conducts P2P energy trading, the comparison between the two schemes is demonstrated in terms of the operation performance of MGs. Figs. 5 and 6 show the distribution of the nodal voltage magnitudes in the interconnected MGs over the entire day using the proposed co-optimization scheme and the benchmark scheme, respectively. It can be observed from Fig. 5 that only considering the P2P energy trading would result in severe under-voltage violations due to the negligence of the network operation. In contrast, all nodal voltage magnitudes are regulated within the secure range (i.e. $0.95 - 1.05$ p.u.) when the P2P energy trading and network operation are jointly considered as shown by Fig. 6. As previously discussed, the phase

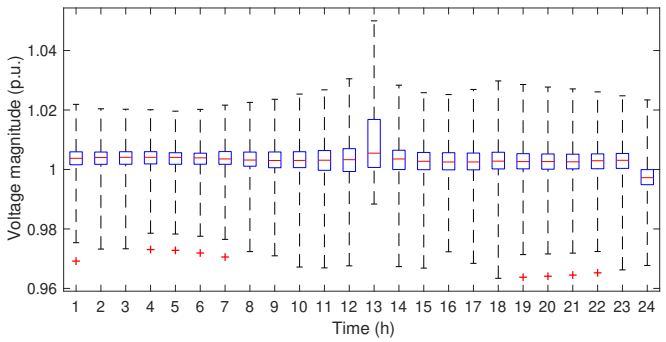


Fig. 6. Distribution of nodal voltage magnitudes under the co-optimization scheme

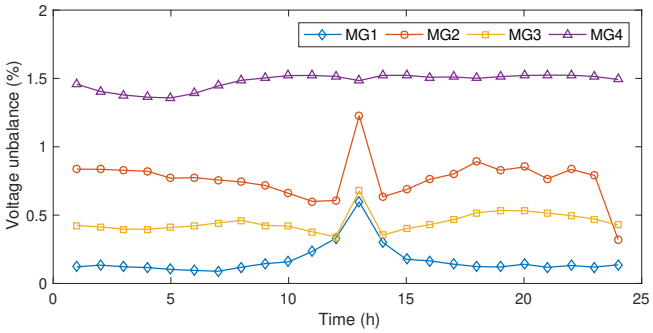


Fig. 8. Profile of the maximum voltage unbalance rate in four MGs considering the three-phase unbalance

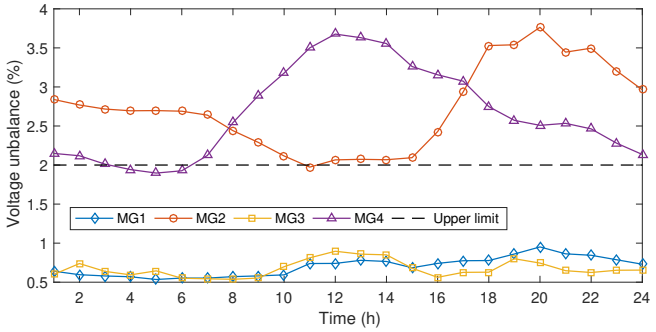


Fig. 7. Profile of the maximum voltage unbalance rate in four MGs ignoring the three-phase unbalance

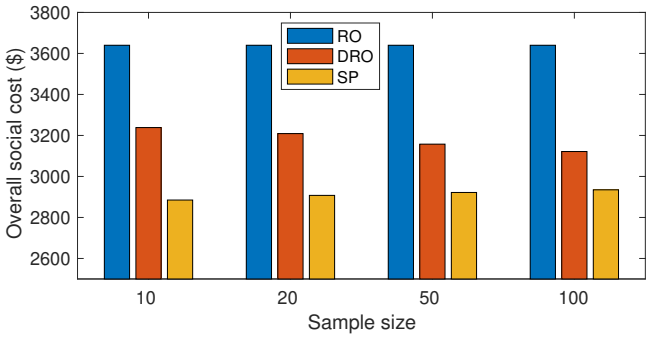


Fig. 9. Comparison of optimal overall social cost using different methods with different sample sizes (ambiguity set with 95% confidence level)

voltage unbalance rate which is defined as the percentage of the maximum phase voltage deviation from the average of the three-phase voltages, should not exceed a certain limit (e.g. 2%) [34]. Figs. 7 and 8 depict the profiles of maximum voltage unbalance rate in all MGs without and with considering the three-phase unbalance of the network, respectively. We can observe from Fig. 7 that when the three-phase unbalance is ignored, MG2 and MG3 would suffer from severe voltage unbalance which would, in turn, cause considerable damage to the three-phase loads such as induction motors. Nevertheless, the voltage unbalance rates in all MGs are maintained well below the upper limit when the three-phase unbalance is considered as shown by Fig. 8. To sum up, our proposed co-optimization scheme is more advantageous than the benchmark scheme in maintaining the network operational security.

### C. Performance Comparison

In this subsection, we compare the performance of our proposed data-driven DRO-based model, denoted as DRO, with three benchmark approaches, i.e., deterministic method denoted as DET, stochastic programming denoted as SP, and robust optimization denoted as RO. Moreover, we demonstrate the relationship between the sample size and solution quality by using sample sets of different sizes in the proposed model. Specifically, four sets are considered with 10, 20, 50, and 100 samples. Another sample set with 5000 samples is used to evaluate the out-of-sample performance.

TABLE II
IN-SAMPLE COST AND OUT-OF-SAMPLE MEAN USING SP AND DRO WITH DIFFERENT SAMPLE SIZES

| Methods | SP | | DRO | |
|---|---|---|---|---|
| Sample size | In-sample cost ($) | Out-of-sample mean ($) | In-sample cost ($) | Out-of-sample mean ($) |
| 10 | 2885.0 | 3016.9 | 3238.4 | 3007.7 |
| 20 | 2907.7 | 2981.0 | 3209.0 | 2980.6 |
| 50 | 2921.9 | 2957.0 | 3157.6 | 2965.7 |
| 100 | 2934.8 | 2950.0 | 3121.6 | 2960.7 |

TABLE III
IN-SAMPLE COST AND OUT-OF-SAMPLE MEAN USING DET AND RO

| Methods | In-sample cost ($) | Out-of-sample mean ($) |
|---|---|---|
| DET | 3231.9 | 5867.0 |
| RO | 3639.9 | 3127.8 |

Fig. 9 shows the optimal values (in-sample costs) of the overall social cost using RO, DRO, and SP with different sample sizes. It is shown that RO yields the highest in-sample cost due to its conservativeness, whereas SP achieves the lowest in-sample cost as it underestimates the true expected cost. The in-sample cost of DRO is significantly lower than that of RO but higher than that of SP as it represents the worst-case expected cost for a given ambiguity set. Furthermore, with the increase in the sample size, the size of the ambiguity set decreases and so does the in-sample cost of DRO. Table II

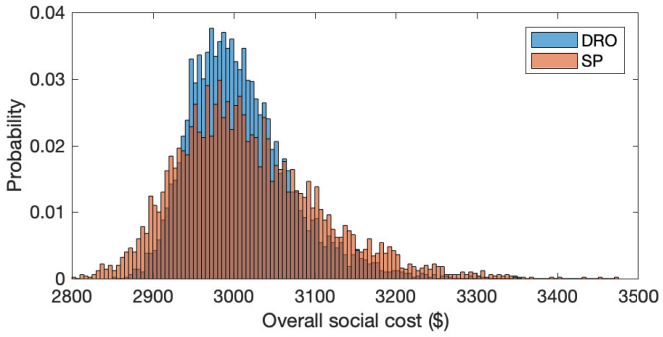


Fig. 10. Out-of-sample distribution of the overall social cost

lists the in-sample costs and the expected out-of-sample cost using SP and DRO. We can observe that for all considered sample sizes, the in-sample costs of SP are optimistically biased as they underestimate the true expected costs that are approximated by the out-of-sample means. With the increase of sample size, the bias in SP is reduced. In contrast, the in-sample cost of DRO provides an upper bound for the out-of-sample cost. Moreover, both the in-sample cost and the expected out-of-sample cost of DRO decline with the increase in the sample sizes. We also compare the computational performance of RO, SP, and DRO. It is shown that RO needs the shortest computational time which is 5.2 seconds per iteration of the ADMM based algorithm. However, RO yields the highest out-of-sample cost as will be shown subsequently. The computational times for DRO and SP are 26.8 and 20.5 seconds per iteration, respectively. Thus, the computational complexity of DRO is quite comparable with SP.

Fig. 10 demonstrates the distribution of the out-of-sample social cost of DRO and SP with 100 in-sample size. Although the difference between the expected social costs is small using DRO and SP, the distribution of the out-of-sample cost using DRO is more concentrated than that using SP. This implies that the solution generated by DRO is more robust compared to that generated using SP. Table III summarizes the in-sample cost and expected out-of-sample cost using DET and RO. We can see that RO has the highest in-sample cost compared to DET and DRO, while DET yields the highest expected out-of-sample cost compared to DRO and RO as it fails to account for the uncertainties. In contrast, the DRO achieves the lowest in-sample cost and out-of-sample mean. Therefore, DRO is less conservative than RO but more robust than SP.

## VI. Conclusion

In this paper, a data-driven DRO model is proposed for the co-optimization of P2P energy trading and network operation in multi-MGs that are interconnected using the flexible SOP technology. Three-phase unbalanced MGs are considered with detailed network constraints. First, a DRO-based energy management model is presented for individual MGs to minimize the operation cost with the given P2P trading prices. Then, a fully decentralized pricing algorithm that achieves the minimum overall social cost is developed. Finally, the Wasserstein metric is used to construct the ambiguity set and the DRO model is converted into an equivalent linear programming problem. The proposed co-optimization scheme of energy trading and network operation is tested in a system with 4 interconnected three-phase unbalanced MGs. The results validate the effectiveness of the proposed scheme and show the improved performance compared to RO and SP-based models.

## References

[1] C. Zhang, Y. Xu, Z. Y. Dong, and J. Ma, "Robust operation of microgrids via two-stage coordinated energy storage and direct load control," *IEEE Trans. on Power Syst.*, vol. 32, no. 4, pp. 2858–2868, 2016.

[2] M. N. Alam, S. Chakrabarti, and A. Ghosh, "Networked microgrids: State-of-the-art and future perspectives," *IEEE Trans. on Ind. Informat.*, vol. 15, no. 3, pp. 1238–1250, 2018.

[3] N. Liu, J. Wang, and L. Wang, "Hybrid energy sharing for multiple microgrids in an integrated heat–electricity energy system," *IEEE Trans. on Sustain. Energy*, vol. 10, no. 3, pp. 1139–1151, 2018.

[4] Z. Zhu, K. W. Chan, S. Bu, B. Zhou, and S. Xia, "Real-time interaction of active distribution network and virtual microgrids: Market paradigm and data-driven stakeholder behavior analysis," *Applied Energy*, vol. 297, p. 117107, 2021.

[5] Z. Wang, B. Chen, J. Wang, M. M. Begovic, and C. Chen, "Coordinated energy management of networked microgrids in distribution systems," *IEEE Trans. on Smart Grid*, vol. 6, no. 1, pp. 45–53, 2014.

[6] Q. Hu, Z. Zhu, S. Bu, K. W. Chan, and F. Li, "A multi-market nanogrid P2P energy and ancillary service trading paradigm: Mechanisms and implementations," *Applied Energy*, vol. 293, p. 116938, 2021.

[7] P. Li, H. Ji, C. Wang, J. Zhao, G. Song, F. Ding, and J. Wu, "Optimal operation of soft open points in active distribution networks under three-phase unbalanced conditions," *IEEE Trans. on Smart Grid*, vol. 10, no. 1, pp. 380–391, 2017.

[8] H. Wang and J. Huang, "Incentivizing energy trading for interconnected microgrids," *IEEE Trans. on Smart Grid*, vol. 9, no. 4, pp. 2647–2657, 2016.

[9] D. Gregoratti and J. Matamoros, "Distributed energy trading: The multiple-microgrid case," *IEEE Trans. on Ind. Electron.*, vol. 62, no. 4, pp. 2551–2559, 2014.

[10] Y. Liu, H. B. Gooi, Y. Li, H. Xin, and J. Ye, "A secure distributed transactive energy management scheme for multiple interconnected microgrids considering misbehaviors," *IEEE Trans. on Smart Grid*, vol. 10, no. 6, pp. 5975–5986, 2019.

[11] N. Liu, M. Cheng, X. Yu, J. Zhong, and J. Lei, "Energy-sharing provider for pv prosumer clusters: A hybrid approach using stochastic programming and stackelberg game," *IEEE Trans. on Ind. Electron.*, vol. 65, no. 8, pp. 6740–6750, 2018.

[12] J. Li, C. Zhang, Z. Xu, J. Wang, J. Zhao, and Y.-J. A. Zhang, "Distributed transactive energy trading framework in distribution networks," *IEEE Trans. on Power Syst.*, vol. 33, no. 6, pp. 7215–7227, 2018.

[13] J. Guerrero, A. C. Chapman, and G. Verbič, "Decentralized P2P energy trading under network constraints in a low-voltage network," *IEEE Trans. on Smart Grid*, vol. 10, no. 5, pp. 5163–5173, 2018.

[14] H. Kim, J. Lee, S. Bahrami, and V. W. Wong, "Direct energy trading of microgrids in distribution energy market," *IEEE Trans. on Power Syst.*, vol. 35, no. 1, pp. 639–651, 2019.

[15] A. Paudel, L. Sampath, J. Yang, and H. B. Gooi, "Peer-to-peer energy trading in smart grid considering power losses and network fees," *IEEE Trans. on Smart Grid*, 2020.

[16] J. R. Birge and F. Louveaux, *Introduction to stochastic programming*. Springer Science & Business Media, 2011.

[17] N. Liu, X. Yu, C. Wang, C. Li, L. Ma, and J. Lei, "Energy-sharing model with price-based demand response for microgrids of peer-to-peer prosumers," *IEEE Trans. on Power Syst.*, vol. 32, no. 5, pp. 3569–3583, 2017.

[18] Z. Guo, P. Pinson, S. Chen, Q. Yang, and Z. Yang, "Chance-constrained peer-to-peer joint energy and reserve market considering renewable generation uncertainty," *IEEE Transactions on Smart Grid*, vol. 12, no. 1, pp. 798–809, 2021.

[19] A. Ben-Tal, L. El Ghaoui, and A. Nemirovski, *Robust optimization*. Princeton University Press, 2009, vol. 28.

[20] Y. Liu, Y. Li, H. B. Gooi, Y. Jian, H. Xin, X. Jiang, and J. Pan, "Distributed robust energy management of a multimicrogrid system in the real-time energy market," *IEEE Trans. on Sustain. Energy*, vol. 10, no. 1, pp. 396–406, 2017.

[21] P. M. Esfahani and D. Kuhn, "Data-driven distributionally robust optimization using the wasserstein metric: Performance guarantees and tractable reformulations," *Mathematical Programming*, vol. 171, no. 1-2, pp. 115–166, 2018.

[22] G. A. Hanasusanto and D. Kuhn, "Conic programming reformulations of two-stage distributionally robust linear programs over wasserstein balls," *Operations Research*, vol. 66, no. 3, pp. 849–869, 2018.

[23] T. Morstyn, A. Teytelboym, C. Hepburn, and M. D. McCulloch, "Integrating P2P energy trading with probabilistic distribution locational marginal pricing," *IEEE Transactions on Smart Grid*, vol. 11, no. 4, pp. 3095–3106, 2020.

[24] C. Wan, J. Lin, J. Wang, Y. Song, and Z. Y. Dong, "Direct quantile regression for nonparametric probabilistic forecasting of wind power generation," *IEEE Transactions on Power Systems*, vol. 32, no. 4, pp. 2767–2778, 2016.

[25] C. Zhao, C. Wan, and Y. Song, "An adaptive bilevel programming model for nonparametric prediction intervals of wind power generation," *IEEE Transactions on Power Systems*, vol. 35, no. 1, pp. 424–439, 2019.

[26] M. Daneshvar, B. Mohammadi-Ivatloo, K. Zare, and S. Asadi, "Two-stage robust stochastic model scheduling for transactive energy based renewable microgrids," *IEEE Transactions on Industrial Informatics*, vol. 16, no. 11, pp. 6857–6867, 2020.

[27] C. Wang, R. Gao, F. Qiu, J. Wang, and L. Xin, "Risk-based distributionally robust optimal power flow with dynamic line rating," *IEEE Trans. on Power Syst.*, vol. 33, no. 6, pp. 6074–6086, 2018.

[28] C. Duan, W. Fang, L. Jiang, L. Yao, and J. Liu, "Distributionally robust chance-constrained approximate AC-OPF with wasserstein metric," *IEEE Trans. on Power Syst.*, vol. 33, no. 5, pp. 4924–4936, 2018.

[29] Y. Guo, K. Baker, E. Dall'Anese, Z. Hu, and T. H. Summers, "Data-based distributionally robust stochastic optimal power flow-part i: Methodologies," *IEEE Trans. on Power Syst.*, vol. 34, no. 2, pp. 1483–1492, 2018.

[30] X. Lu, K. W. Chan, S. Xia, X. Zhang, G. Wang, and F. Li, "A model to mitigate forecast uncertainties in distribution systems using the temporal flexibility of EVAs," *IEEE Trans. on Power Syst.*, vol. 35, no. 3, pp. 2212–2221, 2019.

[31] X. Wu, S. Qi, Z. Wang, C. Duan, X. Wang, and F. Li, "Optimal scheduling for microgrids with hydrogen fueling stations considering uncertainty using data-driven approach," *Applied Energy*, vol. 253, p. 113568, 2019.

[32] R. Zhu, H. Wei, and X. Bai, "Wasserstein metric based distributionally robust approximate framework for unit commitment," *IEEE Trans. on Power Syst.*, vol. 34, no. 4, pp. 2991–3001, 2019.

[33] J. Li, C. Liu, M. E. Khodayar, M.-H. Wang, Z. Xu, B. Zhou, and C. Li, "Distributed online var control for unbalanced distribution networks with photovoltaic generation," *IEEE Transactions on Smart Grid*, vol. 11, no. 6, pp. 4760–4772, 2020.

[34] P. Pillay and M. Manyage, "Definitions of voltage unbalance," *IEEE Power Engineering Review*, vol. 21, no. 5, pp. 50–51, 2001.

[35] J. Wang, N. Zhou, C. Chung, and Q. Wang, "Coordinated planning of converter-based dg units and soft open points incorporating active management in unbalanced distribution networks," *IEEE Transactions on Sustainable Energy*, vol. 11, no. 3, pp. 2015–2027, 2019.

[36] S. Boyd, N. Parikh, E. Chu, B. Peleato, and J. Eckstein, "Distributed optimization and statistical learning via the alternating direction method of multipliers," *Foundations and Trends® in Machine Learning*, vol. 3, no. 1, pp. 1–122, 2011.

[37] P. Zhao, C. Gu, Z. Hu, D. Xie, I. Hernando-Gil, and Y. Shen, "Distributionally robust hydrogen optimization with ensured security and multi-energy couplings," *IEEE Transactions on Power Systems*, 2020.

[38] P. Zhao, C. Gu, Z. Cao, Y. Shen, F. Teng, X. Chen, C. Wu, D. Huo, X. Xu, and S. Li, "Data-driven multi-energy investment and management under earthquakes," *IEEE Transactions on Industrial Informatics*, 2020.

[39] D. T. F. W. Group *et al.*, "Distribution test feeders," *Available from: http://sites.ieee.org/pes-testfeeders/resources*, 2010.


**Jiayong Li** (S'16-M19) received the B.Eng. degree from Zhejiang University, Hangzhou, China, in 2014, and the Ph.D. degree from The Hong Kong Polytechnic University, Hong Kong, in 2018. He is currently an Assistant Professor with the College of Electrical and Information Engineering of Hunan University. He was a Post Doctoral Fellow with the Department of Electrical and Computer Engineering, Southern Methodist University from 2019 to 2020, and was a Visiting Scholar with Argonne National Laboratory in 2017. His research interests include distribution system planning and operation, power economics, demand-side energy management, and distributed control.

**Mohammad E. Khodayar** (SM17) received the B.S. and M.S. degrees in electrical engineering from Amirkabir University of Technology (Tehran Polytechnic) and Sharif University of Technology, respectively; and the Ph.D. degree in electrical engineering from Illinois Institute of Technology, Chicago, IL, USA, in 2012. He was a Senior Research Associate in the Robert W. Galvin Center for Electricity Innovation at Illinois Institute of Technology. He is currently an Associate Professor with the Department of Electrical and Computer Engineering, Southern Methodist University, Dallas, TX, USA. He is the past associate editor of IEEE Transactions on Sustainable Energy and the current associate editor of IEEE Transactions on Vehicular Technology and IEEE Access. His research interests include power system operation and planning, transportation electrification, and applications of machine learning to power systems.

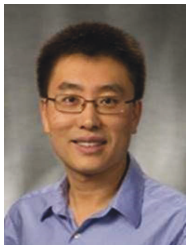

**Jianhui Wang** (M07-SM12-F21) Dr. Jianhui Wang is a Professor with the Department of Electrical and Computer Engineering at Southern Methodist University. Dr. Wang has authored and/or co-authored more than 300 journal and conference publications, which have been cited for more than 30,000 times by his peers with an H-index of 87. He has been invited to give tutorials and keynote speeches at major conferences including IEEE ISGT, IEEE SmartGridComm, IEEE SEGE, IEEE HPSC and IGEC-XI.

Dr. Wang is the past Editor-in-Chief of the *IEEE Transactions on Smart Grid* and an IEEE PES Distinguished Lecturer. He is also a guest editor of a *Proceedings of the IEEE* special issue on power grid resilience. He is the recipient of the IEEE PES Power System Operation Committee Prize Paper Award in 2015, the 2018 Premium Award for Best Paper in IET Cyber-Physical Systems: Theory & Applications, and the Best Paper Award in *IEEE Transactions on Power Systems* in 2020. Dr. Wang is a Clarivate Analytics highly cited researcher for production of multiple highly cited papers that rank in the top 1% by citations for field and year in Web of Science (2018-2020). He is a Fellow of IEEE.

**Bin Zhou** (S11-M13-SM17) was born in Hunan Province, China, in 1984. He received the B.Sc. degree in electrical engineering from Zhengzhou University, Zhengzhou, China, in 2006, the M.S. degree in electrical engineering from South China University of Technology, Guangzhou, China, in 2009, and the Ph.D. degree from The Hong Kong Polytechnic University, Hong Kong, in 2013. Afterwards, he worked as a Research Associate and subsequently a Postdoctoral Fellow in the Department of Electrical Engineering of The Hong Kong Polytechnic University. Now, he is an Associate Professor in the College of Electrical and Information Engineering, Hunan University, Changsha, China. His main fields of research include smart grid operation and planning, renewable energy generation, and energy efficiency.